Proceedings of the Royal Society A, 467 (2011) 234-243

Extraordinary Ductility in Al–bearing δ–TRIP Steel

By H. L. Yi[1], K. Y. Lee[2] and H. K. D. H. Bhadeshia[1,3]

[1]Graduate Institute of Ferrous Technology (GIFT)
Pohang University of Science and Technology (POSTECH)
Pohang 790-784, Republic of Korea

[2]POSCO Technical Research Laboratories
Gwangyang–si, Jeonnam, Republic of Korea

[3]University of Cambridge
Materials Science and Metallurgy, Cambridge CB2 3QZ, U.K.

Abstract

An iron–based alloy system has been developed which exhibits impressive combinations of tensile strength and elongation which are not available with current steels used in the manufacture of automobiles. Furthermore, the heat treatments required to achieve these properties are consistent with practical production processes. The alloys rely on significant concentrations of ferrite–stabilising solutes so that δ–ferrite which forms during solidification is retained in the microstructure.

1. Introduction

There is a huge variety of steels available and many of these result in similar properties but are produced to satisfy particular requirements of cost, weldability, and design criteria (Joo et al., 2009). This overlap of properties is evident also in the formable alloys designed for the automotive industries, although an examination of Fig. 1 shows that the distribution is not uniform; there are significant gaps at intermediate strength and ductility combinations, and when the strength exceeds about 1200 MPa.

There already is research in progress on the stronger steels in order to enhance ductility and assess other engineering properties (Bhadeshia, 2010; Edmonds et al., 2006; Fan et al., 2009; Naderi, 2007). The same attention has not been paid to alloys which have a strength of 600–700 MPa and at the same time exhibit elongations in excess of 30% since these materials are typically formed into components. Although the so–called TWIP † steels fulfil these requirements, they are relatively expensive to manufacture and apply.

† 'TWIP' stands for twinning–induced plasticity, and 'TRIP' for transformation–induced plasticity. Both mechanical twinning and displacive phase transformations have the ability to enhance ductility by delaying the onset of plastic instability during tensile deformation, and hence of ultimate fracture.

TEX Paper

Proceedings of the Royal Society A, 467 (2011) 234-243

It is interesting in this context to explore the recent proposal of δ–TRIP steel in which the alloy is designed to retain a large quantity of δ–ferrite at all temperatures, with the residual microstructure consisting of a mixture of bainitic ferrite and retained austenite (Chatterjee et al., 2007; Yi et al., 2010a,b). The δ–ferrite substitutes for the allotriomorphic ferrite that is normally introduced into TRIP–assisted steels by intercritical annealing or continuous cooling transformation (DeCooman, 2004; Jacques, 2004; Matsumura et al., 1987a,b; Sakuma et al., 1991). There are advantages to this, for example, that a fully martensitic structure cannot be produced in the heat–affected zone of a resistance spot weld. The steel also relies more on aluminium rather than silicon to suppress the formation of cementite, which helps avoid the problem of the adherent fayalite scale (Fukagawa et al., 1994; Okada et al., 1995; Raman, 2006) that forms on the surface during hot–rolling.

The δ–TRIP steel has been demonstrated in the cast state to have an ultimate tensile strength of about 1000 MPa and an elongation of 27% (Chatterjee et al., 2007). Subsequent experiments highlighted the fact that the alloy system is sensitive to non–equilibrium solidification which meant that δ–ferrite could not be reliably retained in the microstructure (Yi et al., 2010a). Further intense research (Yi et al., 2010b) was necessary in order to characterise the transformation behaviour during and after hot–rolling in the two–phase field; the rolling deformation is necessary to apply the steel in sheet form for use in the manufacture of automobiles. In the present work we report for the first time, some exciting mechanical property data for what we believe is a complete alloy design of a type consistent with large–scale manufacture.

2. Alloys and Experimental Method

The alloy design procedures involving phase diagram calculations have been detailed elsewhere (Chatterjee et al., 2007; Yi et al., 2010a,b) and are not repeated here. They basically help ensure the presence of δ–ferrite under equilibrium conditions, at all temperatures in the solid state. Aluminium plays a key role in this and experience based on experiments (Yi et al., 2010a) has indicated that such calculations overestimate the amount of δ–ferrite expected when the real alloys solidify during casting under conditions which deviate from equilibrium. Therefore, the two alloys studied here (Table 1) have larger aluminium concentrations than in the original work (Chatterjee et al., 2007).

The alloys were manufactured as 34 kg ingots $100 \times 170 \times 230$ mm size using a vacuum melting furnace. The ingots were reheated to 1200°C for rough rolling to make 25–30 mm slabs followed by air cooling. These slabs were then reheated to 1200°C and hot–rolled to 3 mm in thickness; 1.2 mm thick sheets were then produced by cold rolling. The heat treatments outlined in Table 2 were conducted using $1.2 \times 40 \times 110$ mm samples in a CCT–Ay (Ulvac–RIKO) simulator where the samples were heated at $20^{\circ}\mathrm{C\,s^{-1}}$ in a nitrogen atmosphere to allow some austenite to form, followed by cooling at $-20^{\circ}\mathrm{C\,s^{-1}}$ to the temperature where bainitic ferrite is allowed to form, and finally at $-10^{\circ}\mathrm{C\,s^{-1}}$ to ambient temperature. Samples for tensile tests were machined from these blanks to ASTM standard E8M–00 with elongation measured on a 10 mm gauge length over the 25 mm parallel length, following tension at $3.3 \times 10^{-3}\,\mathrm{s^{-1}}$. All the mechanical data presented in this pa-

per represent the average of three tests; the reproducibility was excellent with the elongation varying by no more than ±2% and the strength by ±5 MPa.

Microstructural evolution was studied using samples $2\times3\times10$ mm on a dilatometer described elsewhere (Pak et al., 2008). X–ray diffraction was done on metallographically prepared samples etched using 2% nital in order to remove any deformed surface, with Cu K_α radiation with the data subjected to Rietveld analysis (Hill and Howard, 1987) and refinement (Rietveld, 1967, 1969). The austenite lattice parameter thus obtained was used to estimate the concentration of carbon using a published equation (Dyson and Holmes, 1970).

Most phases could easily be identified using scanning electron microscopy. The austenite regions stand proud of the surface, and the bainite is in the form of sheaves which appear at these magnifications as plates. The δ–ferrite is given away by its coarse scale whereas the allotriomorphic ferrite appears as finer equiaxed grains. Pearlite present in the hot–rolled samples (without subsequent heat treatment) appears with dark contrast because the cementite and ferrite phases are intimately mixed. Martensite that forms during deformation could not be resolved but its presence is deduced from the decrease in the retained austenite content as measured using X–ray diffraction.

3. Microstructure

The microstructures of the alloys in the hot–rolled condition are illustrated in Fig. 2a,b, where we distinguish δ–ferrite and α–ferrite simply to identify the former as having been retained from solidification and has persisted through the hot–deformation, whereas the α is a result of transformation from austenite. None of the δ–ferrite is retained in the microstructure of Alloy 8 which becomes fully austenitic during hot–rolling, resulting in a final microstructure of equiaxed grains of α and somewhat discontinuous pearlite. In contrast, Alloy 9 which contains more aluminium and less manganese, has the coarse elongated regions of ferrite which represent the δ phase. The influence of composition is also reflected in the quantitative data given in Table 2 where the total fraction of $(\delta+\alpha)$ is seen to be greater in Alloy 9 in the hot–rolled condition.

Metallography was conducted on all of the heat–treated samples listed in Table 2 but only a few representative results are illustrated in Fig. 2c,d for the particular case where the intercritical anneal was at 850°C followed by isothermal transformation at 400°C for 600 s. For the discussion below, the terms $V_{\rm HR}$ and $V_{\rm IA}$ represent the fractions of $(\delta+\alpha)$ ferrite present in the microstructure in the hot–rolled and intercritically annealed conditions respectively.

Alloy 8 following heat treatment consists of fine and equiaxed allotriomorphic ferrite grains together with islands of retained austenite containing regions of bainitic ferrite. The intercritical annealing temperature is not high enough to fully austenitise the material so the total fraction of allotriomorphic ferrite has decreased only a little from $V_{\rm HR}=0.71\pm0.09$ in the hot–rolled state to $V_{\rm IA}=0.66\pm0.07$ – this general observation is essentially correct for both alloys and intercritical annealing temperatures studied, as can be seen in Table 2. Retained austenite measurements are discussed in the next section.

Alloy 9 differs in that there is a mixture of the δ–ferrite together with allotriomorphic ferrite; the overall fraction of ferrite is larger by about 0.1 volume fraction,

as expected from the composition difference relative to Alloy 8 (Table 2). The quantity of bainite within the retained austenite is also much smaller, because of the greater stabilisation of the residual austenite by carbon partitioned from the ($\delta+\alpha$). Most of the islands of austenite were featureless at high magnification, Fig. 2d.

4. Deformation

A summary of the mechanical properties obtained is presented in Fig. 3 with the details listed in Table 2. The strength–elongation combination is impressive for all the heat–treatments applied, and approaches that of the high–Mn TWIP steels (Frommeyer et al., 2003; Grässel et al., 2000) which are more challenging to produce and apply. The data also fall in a domain which is not occupied by other automotive steels and furthermore, the ductility is comparable to that of the much weaker interstitial–free steels (Bayraktar et al., 2007; Hayat et al., 2009; Mukhopadhyay et al., 2009). The alloy also outperforms TRIP and dual–phase steels at the same strength level.

One reason for the large ductility observed is the presence of retained austenite in a form which transforms during deformation but has a stability which means that the transformation is gradual so that local stress concentrations which lead to damage can be accommodated to large strains Bhadeshia (2008); Chatterjee et al. (2007). Fig. 4 shows clearly that both the harder austenite (Furnemont et al., 2002) which also contains the bainite, and the allotriomorphic and δ–ferrite deform in a compatible manner until final fracture occurs; the micrographs are taken in the close proximity ($\simeq 1\,\mathrm{mm}$) of the fracture surface and illustrate the elongation experienced by all the phases present.

Fig. 5 shows the quantitative measurements of retained austenite both before and after deformation and it is evident that the austenite is reasonably stable given the large extent of plastic strain. The data also show that the austenite fraction is smaller in the case of Alloy 9, and its carbon concentration larger. This is because it contains a greater aluminium and lower manganese concentration than Alloy 8, which means that a larger amount of ferrite is present at the intercritical annealing temperature (86% compared with the 71% in Alloy 8). The residual austenite is therefore enriched to a correspondingly greater degree due to the partitioning of carbon between the ferrite and austenite.

It should also be noted that the stability of the austenite increases if it survives the initial plastic strains and stresses, because the defect structure introduced during deformation can mechanically stabilise it to martensitic transformation (Chatterjee et al., 2006; Fiedler et al., 1955; Leslie and Miller, 1964; Machlin and Cohen, 1951).

Alloy 8 in general shows better ductility than Alloy 9, presumably because of its finer structure. As pointed our earlier, the former becomes fully austenitic during hot–rolling so that the coarse regions of δ–ferrite which exist in Alloy 9 are absent. Even though Alloy 8 in its final state does not fit the general concept of δ–TRIP steels, the work suggests that the properties of steels which do retain the δ–ferrite could be improved by refining this phase. This could be achieved by controlling the solidification rate or by enhanced deformation during hot–rolling. This latter procedure would be practical when dealing with large castings than in the present work where small quantities of experimental alloys were fabricated.

Tensile curves for Alloy 8 are illustrated in Fig. 6 showing a form consistent with the requirements of automotive steels; the small initial elongation at constant stress did not lead to any observable Lüders bands on the tensile specimen surfaces. It is not clear whether this would become an issue in the context of industrial production as opposed to the present laboratory experiments. Notice also the excellent reproducibility of the tests.

A detailed examination of the tensile data (Table 2) shows that the time at the isothermal transformation temperature does not significantly influence the mechanical properties, probably because the amount of bainite produced is rather small given the large carbon concentration of the austenite. It would be interesting in future work to eliminate the isothermal step altogether and assess the resulting properties.

5. Summary

A novel alloy system based on the concept of stabilising ferrite in the microstructure using aluminium as an alloying element has been found to exhibit promising combinations of tensile strength and elongation. These properties fall in a domain which is not represented by other commercially available or experimental steels designed for the automobile production.

The heat–treatments necessary to achieve the microstructure involve intercritical annealing followed by isothermal transformation at temperatures and time periods which are consistent with large scale production on the so–called continuous annealing facilities (Yanagishima et al., 1983). The isothermal transformation can even be conducted at 450°C which is compatible with a final galvanising treatment.

In future work it is hoped to investigate the spot–welding characteristics; the key feature of the alloy design in this respect is that δ–ferrite can be retained permanently in the microstructure so that fully martensitic regions are not produced in the heat–affected zone of the spot weld.

Acknowledgments

We acknowledge Professor Hae–Geon Lee for the provision of laboratory facilities at GIFT, and support from POSCO through the Steel Innovation Programme. The authors are also grateful for support from the World Class University Programme of the National Research Foundation of Korea, Ministry of Education, Science and Technology, project number R32–2008–000–10147–0.

References

Bayraktar, E., Kaplan, D., Devillers, L., Chevalier, J. P., 2007. Grain growth mechanism during the welding of interstitial free (IF) steels. Journal of Materials Processing Technology 189, 114–125.

Bhadeshia, H. K. D. H., 2001. Bainite in Steels, 2nd edition. Institute of Materials, London.

Bhadeshia, H. K. D. H., 2008. Properties of fine–grained steels generated by displacive transformation. Materials Science and Engineering A 481–482, 36–39.

Bhadeshia, H. K. D. H., 2010. Nanostructured bainite. Proceedings of the Royal Society of London A 466, 3–18.

Chatterjee, S., Murugananth, M., Bhadeshia, H. K. D. H., 2007. δ–TRIP steel. Materials Science and Technology 23, 819–827.

Chatterjee, S., Wang, H. S., Yang, J. R., Bhadeshia, H. K. D. H., 2006. Mechanical stabilisation of austenite. Materials Science and Technology 22, 641–644.

DeCooman, B., 2004. Structure–properties relationship in TRIP steels containing carbide-free bainite. Current Opinion in Solid State and Materials Science 8, 285–303.

Dyson, D. J., Holmes, B., 1970. Effect of alloying additions on the lattice parameter austenite. Journal of the Iron and Steel Institute 208, 469–474.

Edmonds, D. V., He, K., Rizzo, F. C., Cooman, B. C. D., Matlock, D. K., Speer, J. G., 2006. Quenching and partitioning martensite – a novel steel heat treatment. Materials Science & Engineering A 438–440, 25–34.

Fan, D. W., Kim, H. S., Cooman, B. C. D., 2009. Review of the physical metallurgy related to hot press forming of advanced high strength steel. Steel Research International 80, 241–248.

Fiedler, H. C., Averbach, B. L., Cohen, M., 1955. The effect of deformation on the martensitic transformation. Transactions of the American Society for Metals 47, 267–290.

Frommeyer, G., Brüx, U., Neumann, P., 2003. Supra-ductile and high-strength manganese–TRIP/TWIP steels for high energy absorption purposes. ISIJ International 43, 438–446.

Fukagawa, T., Okada, H., Maehara, Y., 1994. Mechanism of red scale defect formation in Si–added hot–rolled steel sheets. ISIJ International 34, 906–911.

Furnemont, Q., Kempf, M., Jacques, P. J., Göken, M., Delannay, F., 2002. On the measurement of the nanohardness of the constitutive phases of TRIP–assisted multiphase steels. Materials Science and Engineering A 328A, 26–32.

Grässel, O., Kruger, L., Frommeyer, G., Meyer, L. W., 2000. High strength Fe–Mn–(Al, Si) TRIP/TWIP steels development—properties—application. International Journal of Plasticity 16, 1391–1409.

Hayat, F., Demir, B., Acarer, M., Aslanar, S., 2009. Effect of weld time and weld current on the mechanical properties of resistance spot welded IF (DIN EN 10130–1999) steel. Kovove Materialy 47, 11–17.

Hill, R. J., Howard, C. J., 1987. Quantitative phase analysis from neutron powder diffraction data using the Rietveld method. Journal of Applied Crystallography 20, 467–487.

Jacques, P. J., 2004. Transformation-induced plasticity for high strength formable steels. Current Opinion in Solid State and Materials Science 8, 259–265.

Joo, M. S., Ryu, J. H., Bhadeshia, H. K. D. H., 2009. Domains of steels with identical properties. Materials and Manufacturing Processes 24, 53–58.

Leslie, W. C., Miller, R. L., 1964. The stabilization of austenite by closely spaced boundaries. ASM Transactions Quarterly 57, 972–979.

Machlin, E. S., Cohen, M., 1951. Burst phenomenon in the martensitic transformation. Trans. Metall. Soc. AIME 191, 746–754.

Matsumura, O., Sakuma, Y., Takechi, H., 1987a. Enhancement of elongation by retained austenite in intercritical annealed 0.4C-1.5Si-0.8Mn steel. Transactions of the Iron and Steel Institute of Japan 27, 570–579.

Matsumura, O., Sakuma, Y., Takechi, H., 1987b. TRIP and its kinetic aspects in austempered 0.4C-1.5Si-0.8Mn steel. Scripta Metallurgica 27, 1301–1306.

Mukhopadhyay, G., Bhattacharya, S., Ray, K. K., 2009. Strength assessment of spot-welded sheets of interstitial free steels. Journal of Materials Processing Technology 209, 1995–2007.

Naderi, M., 2007. Hot stamping of ultra–high strength steels. Ph.D. thesis, RWTH Aachen, Germany.

Okada, H., Dukagawa, T., Okamoto, A., Azuma, M., Matsuda, Y., 1995. Prevention of red scale formation during hot rolling of steels. ISIJ International 35, 886–891.

Pak, J. H., Bhadeshia, H. K. D. H., Karlsson, L., Keehan, E., 2008. Coalesced bainite by isothermal transformation of reheated weld metal. Science and Technology of Welding and Joining 13, 593–597.

Raman, R. K. S., 2006. Characterisation of 'rolled-in', 'fragmented' and 'red' scale formation during secondary processing of steels. Engineering Failure Analysis 13, 1044–1050.

Rietveld, H. M., 1967. Line profiles of neutron powder-diffraction peaks for structure refinement. Acta Crystallographica 22, 151–152.

Rietveld, H. M., 1969. A profile refinement method for nuclear and magnetic structures. Journal of Applied Crystallography 2, 65–71.

Sadagopan, S., Wong, C., Huang, M., Yan, B., Urban, D., 2003. Formability characterisation of new generation of high strength steels. Tech. Rep. TRP 0012, American Iron and Steel Institute, Pittsburgh, USA.

Sakuma, Y., Matsumura, O., Takechi, H., 1991. Mechanical-properties and retained austenite in intercritically heat-treated bainite-transformed steel and their variation with Si and Mn additions. Metallurgical & Materials Transactions A 22, 489–498.

Yanagishima, F., Nakazato, Y., Shimoyama, Y., Sunami, H., Ida, Y., Haga, T., Irie, T., 1983. Development of a multipurpose continuous annealing line for cold rolled sheet steel. Iron and Steel Engineer 60, 36–44.

Yi, H. L., Ghosh, S. K., Liu, W. J., Lee, K. Y., Bhadeshia, H. K. D. H., 2010a. Nonequilibrium solidification and ferrite in δ–TRIP steel. Materials Science and Technology 26, DOI 10.1179/174328409X428918.

Yi, H. L., Lee, K. Y., Bhadeshia, H. K. D. H., 2010b. Stabilisation of ferrite in hot-rolled in δ–TRIP steel. Materials Science and Technology 26, DOI 10.1179/026708309X12506934374001.

Table 1. Chemical compositions (wt%) of the alloys studied. The alloy designations are maintained identical to previous work (Yi et al., 2010a) in order to avoid confusion.

	C	Si	Mn	Al
Alloy 8	0.40	0.22	1.03	2.95
Alloy 9	0.39	0.21	0.51	3.84

Table 2. Intercritical annealing and isothermal transformation heat treatments implemented on simulator. T and t stand for temperature and time respectively, V_{HR} and V_{IA} the fractions of $(\delta + \alpha)$ ferrite present in the microstructure in the hot–rolled and intercritically annealed conditions respectively. The values of V_{HR} for Alloys 8 and 9 are 0.71 ± 0.09 $(2562\,\mu\mathrm{m}^2)$ and 0.86 ± 0.02 $(2562\,\mu\mathrm{m}^2)$ respectively. The areas indicated in brackets after each volume fraction refers to that examined for the volume fraction measurements made using point counting on scanning electron micrographs. ε_U and ε_T stand for uniform and total elongations in percent, respectively, and UTS for the ultimate tensile strength.

Intercritical		Isothermal		Alloy 8	Alloy 9	Alloy 8			Alloy 9		
T / °C	t / s	T / °C	t / s	V_{IA}	V_{IA}	ε_U	ε_T	UTS / MPa	ε_U	ε_T	UTS / MPa
850	180	350	1200	0.66 ± 0.07 $(2562\,\mu\mathrm{m}^2)$	0.77 ± 0.08 $(33642\,\mu\mathrm{m}^2)$	28	37	710	28	37	647
		400	600			34	43	709	31	41	648
		450	120			33	40	740	32	41	661
950	180	350	1200	0.69 ± 0.05 $(15540\,\mu\mathrm{m}^2)$	0.75 ± 0.07 $(15540\,\mu\mathrm{m}^2)$	25	34	711	26	38	639
		400	300			29	37	712	30	40	639
		400	600			30	39	688	30	41	622
		400	900			29	38	693	29	40	629
		450	120			30	38	725	31	40	649

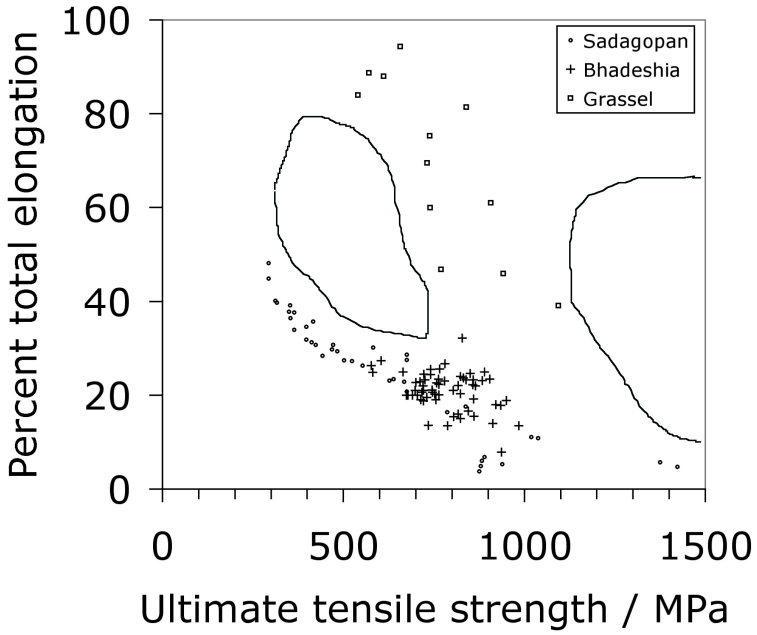

Figure 1. An illustration of the range of strength and elongation combinations available for automotive steels; data compiled from Sadagopan *et al.* (Sadagopan et al., 2003) on TRIP–assisted, dual phase, interstitial-free steels, from Grässel *et al.* TWIP steels (Grässel et al., 2000) and from Bhadeshia on TRIP–assisted steels (Bhadeshia, 2001). Two domains are marked indicating combinations of properties which are not readily accessible.

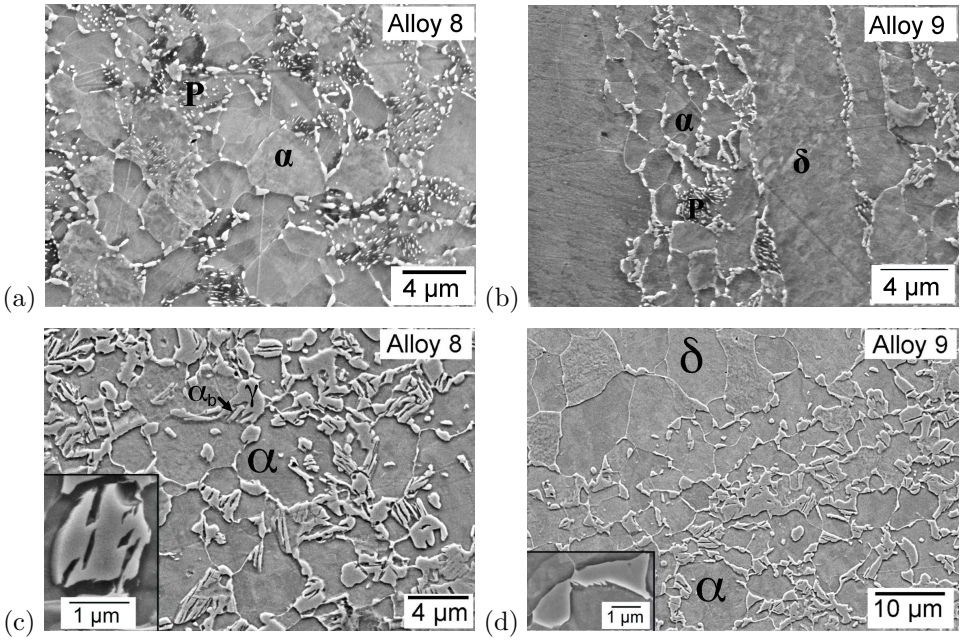

Figure 2. (a) Mixture of allotriomorphic ferrite (α) and pearlite obtained in Alloy 8 following hot–rolling. (b) Mixture of recrystallised δ–ferrite, α and pearlite in hot–rolled Alloy 9. (c,d) Corresponding microstructures following heat treatment for the samples illustrated in (c,d) consisting of an intercritical anneal at 850°C followed by isothermal holding at 400°C for 600 s. The pearlite has now been eliminated and both microstructures have retained austenite. Plates of bainite (α_b) are visible in association with the austenite. Note that (d) is presented at a lower magnification to show that the relatively featureless region on the top–left corresponds to retained δ–ferrite.

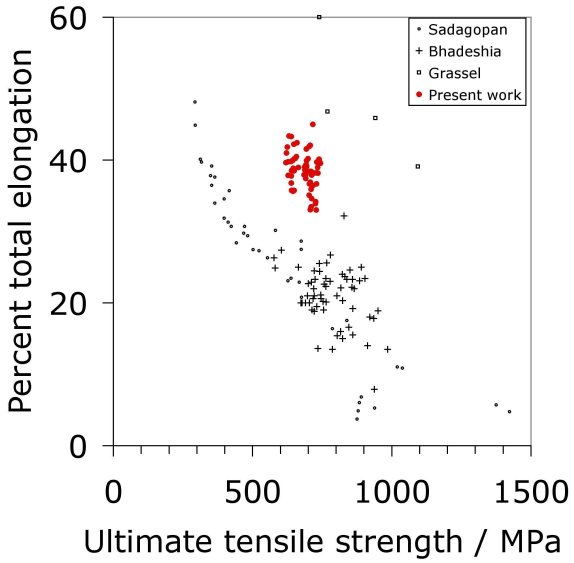

Figure 3. Summary of the mechanical properties obtained (demarcated data) in the context of published data (which are also illustrated in Fig. 1).

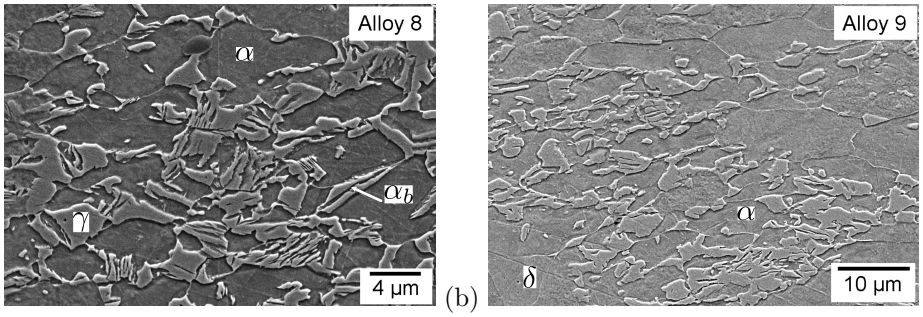

(a) (b)

Figure 4. Micrographs taken from broken tensile specimens at locations about 1 mm away from the fracture surface. The samples were intercritically annealed at 850°C followed by isothermal transformation at 400°C for 600 s. (a) Alloy 8. (b) Alloy 9. Martensite is present in both of these samples as deduced from the X–ray diffraction data, but is in a fine state and not easily identified in these images.

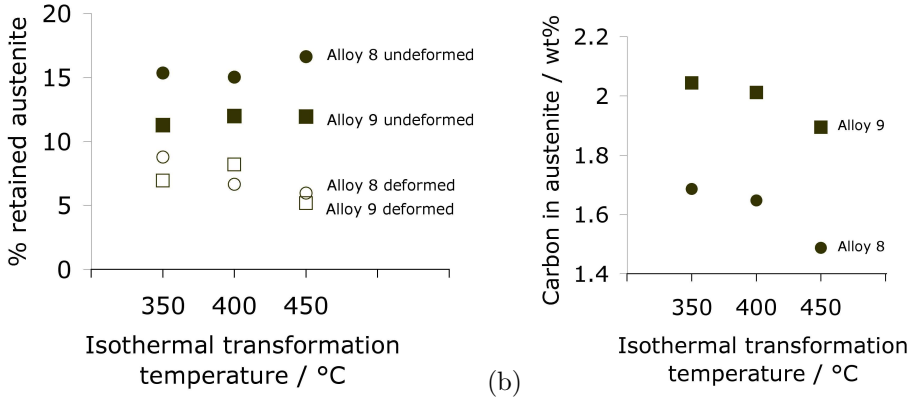

(a) (b)

Figure 5. Data for samples intercritically annealed at 850°C followed by isothermal transformation at the temperature indicated. (a) Retained austenite (with a maximum error of ±0.30% for 95% confidence). (b) Carbon concentration in the retained austenite.

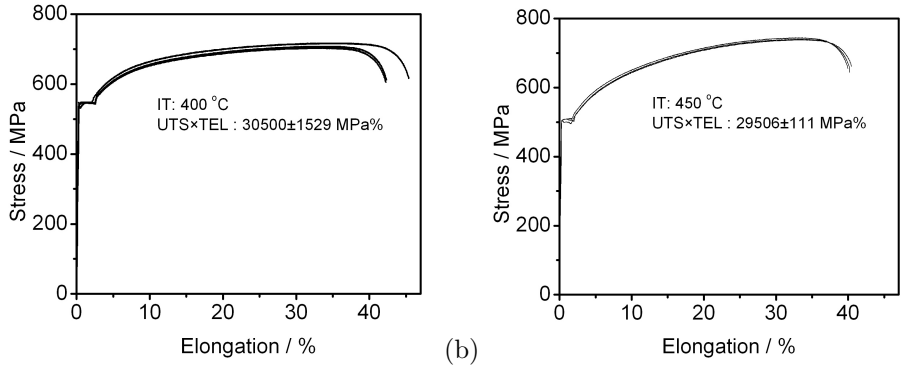

(a) (b)

Figure 6. Typical tensile test data for Alloy 8 intercritically annealed at 850°C for 180 s followed by isothermal transformation at (a) 400°C for 600 s and (b) 450°C for 600 s.